Delft University of Technology

Lifting line model of a wind turbine

Rotor wake aerodynamics assignment 2

Changkyu Park 4646061
Cihangir Özbek 4448146
Malte Wegener 4672194

Submission Date: May 31, 2021
Course: AE4135
Group: 25

Contents

1. Introduction

To perform a higher fidelity performance estimation of a wind turbine than what is achieved with a blade element momentum method (BEM), a lifting line method is employed. This method also enables the performance calculations of multiple rotors placed in the vicinity of each other.

The report first presents an outline of the code that was written to calculate rotor performance. Furthermore, the main assumptions made in constructing the model are stated. The code is then used and the performance of an isolated rotor is compared to the performance of 2 rotors placed next to each other at different distances and also at different phase differences. In the next section, the results of the lifting line method are compared to the blade element method. In the second to last section, the sensitivity of the code is assessed concerning different discretization parameters. The results are then summarised in the conclusion of the report.

2. Implementation and Assumptions

The code is implemented into python and is structured according to the flowchart in Figure 1. Two levels of iteration are performed to converge both the circulation of the blades as well as to converge the average induction, which dictates the shape of the frozen wake. The performance of each blade is section is calculated from the relative airflow angle and velocity, using a pre-computed airfoil polar. This approach does not take into account variation of Reynolds number over the span due to a change in the chord or relative flow velocity. The wake is advected with a uniform speed, which is determined by the average induction factor of the rotor. This approach does not take into account the effect the wake has on itself, thus ignoring the variation of axial velocity in the radial direction. Furthermore, the viscous dissipation of vorticity is ignored and the flow is assumed to be completely inviscid.

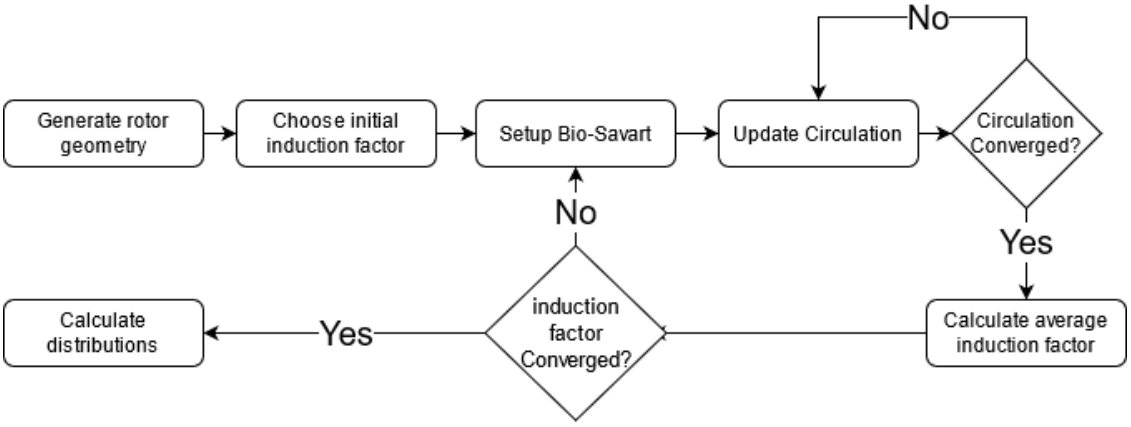

Fig. 1 Flowchart of the code

3. Comparison between single and double rotor cases

In this section, the results of the simulation for the single and double rotor cases are compared. These include the radial distribution of various parameters and the total thrust and power coefficients. For the double rotor cases that have two rotors in-plane, various distances L from each other are considered and they are $L = D, 2D, 5D, 50D$ where D is the diameter of the rotor. For power coefficient analysis $L = 250D$ has also been considered to achieve convergence. Furthermore, the effect of the rotational phase difference between the rotors for the double rotor cases is analysed using various phase shift $\psi = 0, \pi/2, \pi, 3\pi/2$ at a distance $L = D$ between the two rotors. To present clear similarity or difference observations, only one of the two rotors for the double rotor case will be plotted together with the single rotor case for figures relevant to the radial distribution.

3.1. Radial distribution of the angle of attack

Firstly, the radial distributions of the angle of attack α for the 5 different cases are presented in Figure 2. It can be observed from the plot that the distribution does not vary significantly, especially towards the tip of the rotor. It varies minimally near the hub and this difference reduces quickly with an increase in L. Already from $L = 2D$, the plot almost

overlaps the single rotor case and for even greater values of L, it can be realised that they completely overlap the single rotor case.

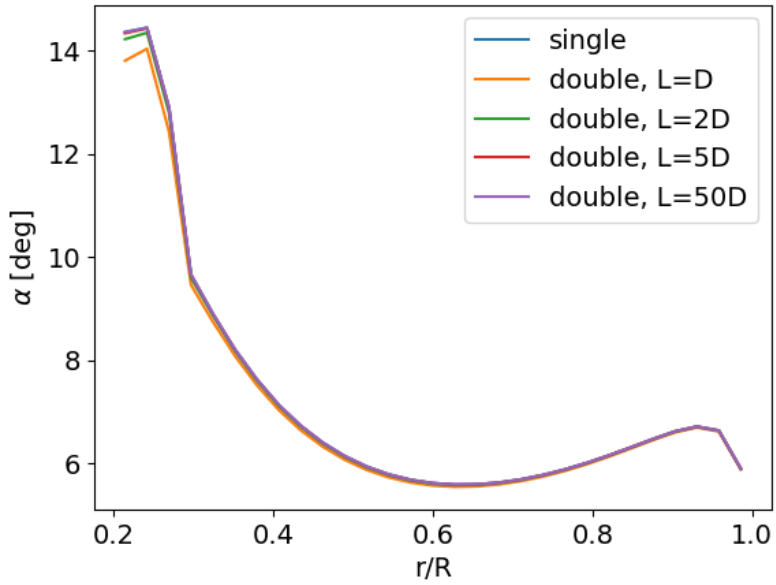

Fig. 2 Comparison of radial distribution of angle of attack for single and double rotor cases for various L at $\psi = 0$

Similarly, the effect of various values of ψ at $L = D$ was analysed for α as shown in Figure 3. It is to be noted that all of the curves that represent the double rotor cases overlap and it is thus presented as a single purple curve in the plot. It could hence be realised that the phase difference between the two rotors in the double rotor case does not affect α.

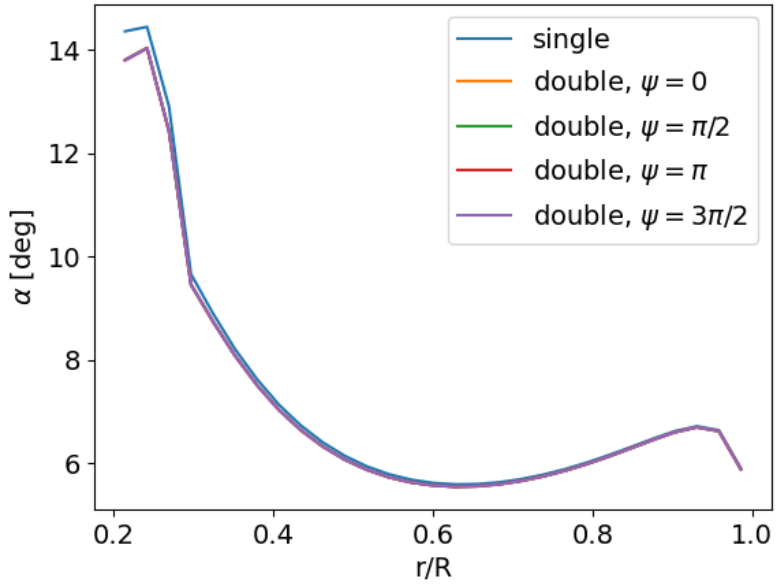

Fig. 3 Comparison of radial distribution of angle of attack for single and double rotor cases for various ψ at $L = D$

It was expected that a further increase in L would not impose any changes to the radial distribution of α as it could be inferred from Figure 2 and Figure 3 which showed that non-zero phase differences ψ have no significant effect in α and thus a further increase in L would merely follow the result of Figure 2. However, the result for non-zero ψ has been produced at $L = 2D$ as shown in Figure 4 to double-check this assumption.

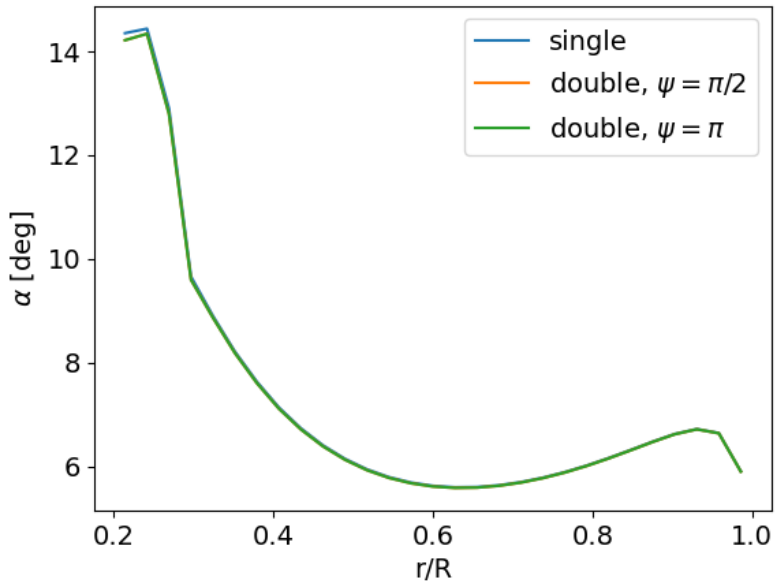

Fig. 4 Comparison of radial distribution of angle of attack for single and double rotor cases for various ψ at $L = 2D$

Without any surprise, the result exactly corresponded to the aforementioned assumption.

3.2. Radial distribution of inflow angle

As for the inflow angle ϕ, similar conclusion can be drawn as it was done for the angle of attack from Figure 5. There is minimal difference from the single rotor case for the double rotor case of low L near the hub but towards the tip, this difference completely vanishes.

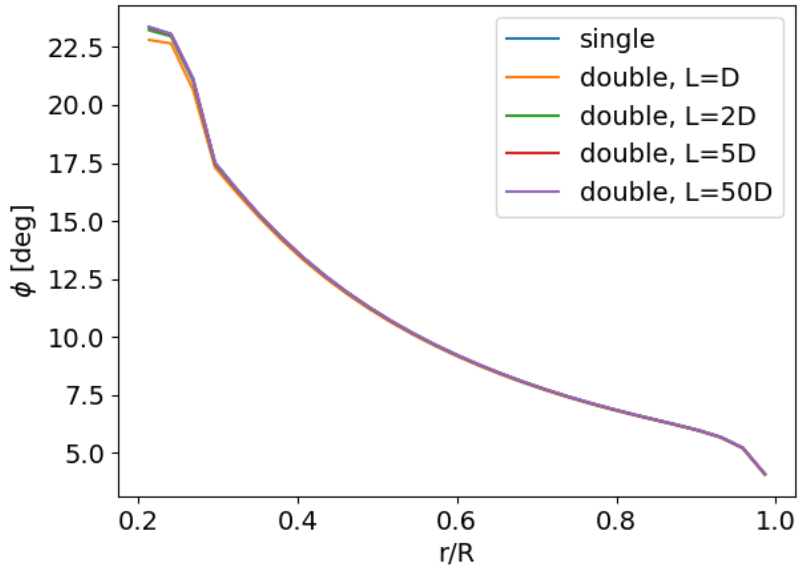

Fig. 5 Comparison of radial distribution of inflow angle for single and double rotor cases for various L at $\psi = 0$

Again, the effect of the phase difference between the two rotors has been portrayed in Figure 6 for various values of ψ and a similar conclusion can be made as it was done for α. All the double rotor cases' curves overlap and thus there is no effect of the phase difference on ϕ.

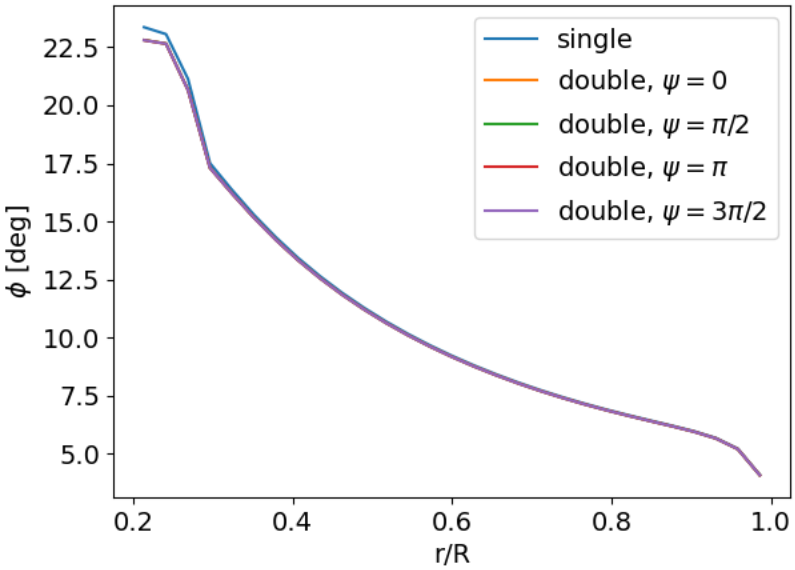

Fig. 6 Comparison of radial distribution of inflow angle for single and double rotor cases for various ψ at $L = D$

Due to the small difference between the single rotor and double rotor cases at $L = D$ and the non-significant effect of phase differences ϕ, it was again checked for a higher value of L at $L = 2D$ whether it truly followed the trend of Figure 5 where the double rotor case approaches single rotor case for increasing L. The plot of Figure 7 was then plotted to support this pre-made assumption.

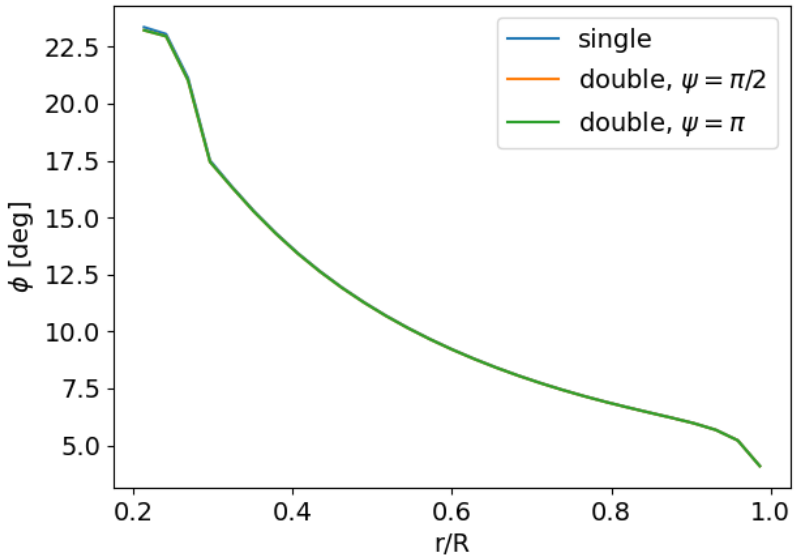

Fig. 7 Comparison of radial distribution of inflow angle for single and double rotor cases for various ψ at $L = 2D$

Highly similar to the conclusion made for α, phase differences ψ still have no effect on ϕ even at higher L of $2D$.

3.3. Radial distribution of circulation

The radial distribution of dimensionless circulation is also plotted in Figure 8. The dimensionless circulation is calculated as

$$\Gamma_{\text{dimensionless}} = \frac{\Gamma}{U_\infty^2 \pi} B\Omega \tag{3.1}$$

where U_∞ is the freestream velocity, B is the number of blades and Ω is the rotational speed of rotor in [rad/s]. Just like the previous 2 radial distributions, circulation of the double rotor case at small value of L differs slightly from the single rotor case only near the hub and as the value of L is increased, there is no observable difference.

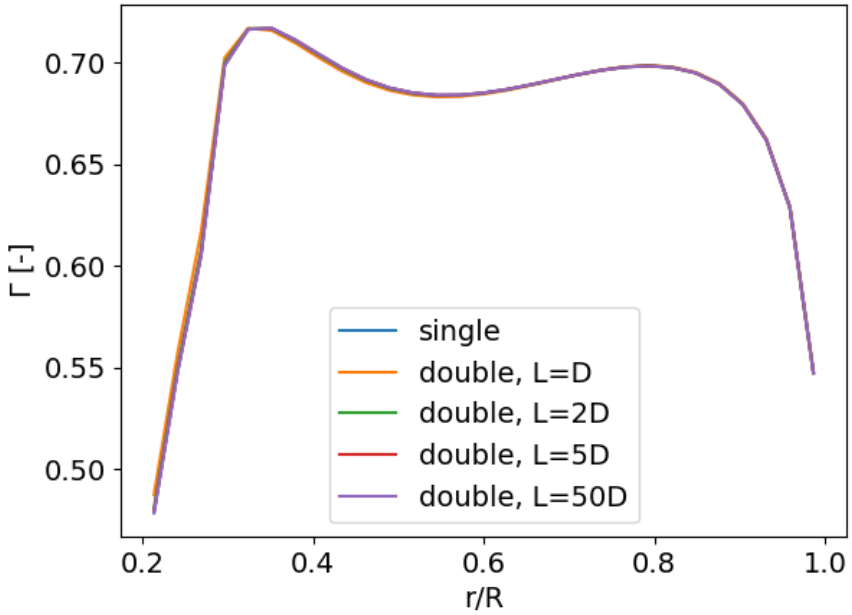

Fig. 8 Comparison of radial distribution of circulation for single and double rotor cases for various L at $\psi = 0$

Another exactly same conclusion can be made for the effect of the phase difference between the two rotors for the double rotor cases as it was made for its effect on α and ϕ. There is absolutely no difference in the curves of the double rotor cases as shown in Figure 9.

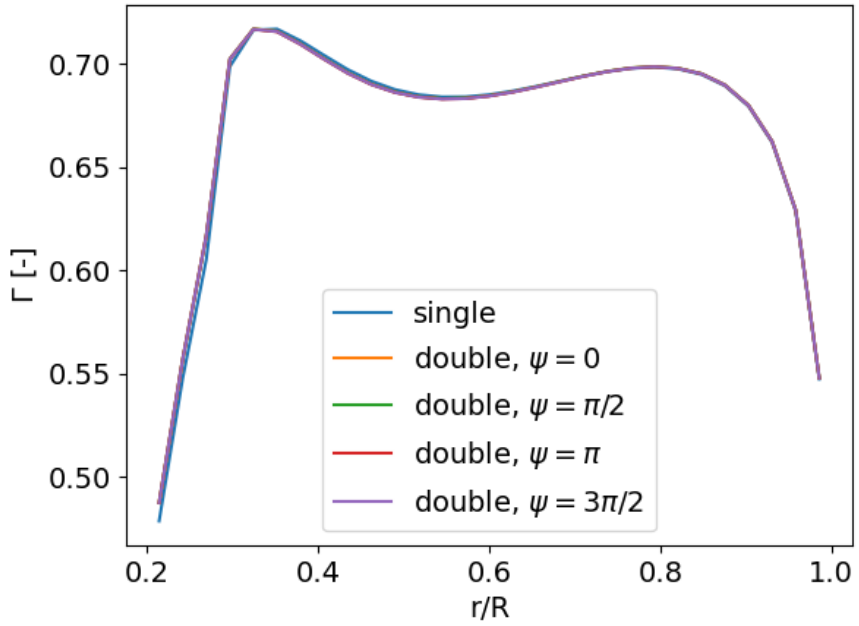

Fig. 9 Comparison of radial distribution of circulation for single and double rotor cases for various ψ at $L = D$

3.4. Radial distribution of loads

The radial distribution of tangential load and axial load are presented in Figure 10 and Figure 11 respectively. The dimensionless forces are calculated as

$$\text{Tangential force coefficient} = \frac{F_t}{\frac{1}{2}\rho U_\infty^2 R} \tag{3.2}$$

$$\text{Axial force coefficient} = \frac{F_a}{\frac{1}{2}\rho U_\infty^2 R} \tag{3.3}$$

where F_t and F_a are dimensional tangential and axial forces respectively, ρ is the air density and R is the radius of the rotor. For both plots, it can be observed that the results for double rotor cases are almost inline with the single rotor case regardless of the magnitude of L. Thus, it can be concluded that additional rotor in plane does not have a significant effect on the radial distribution of forces.

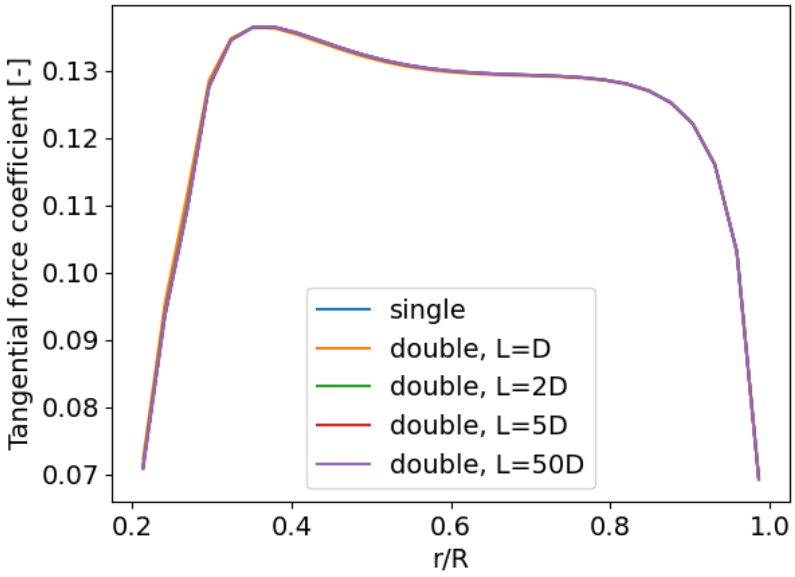

Fig. 10 Comparison of radial distribution of tangential load for single and double rotor cases for various L at $\psi = 0$

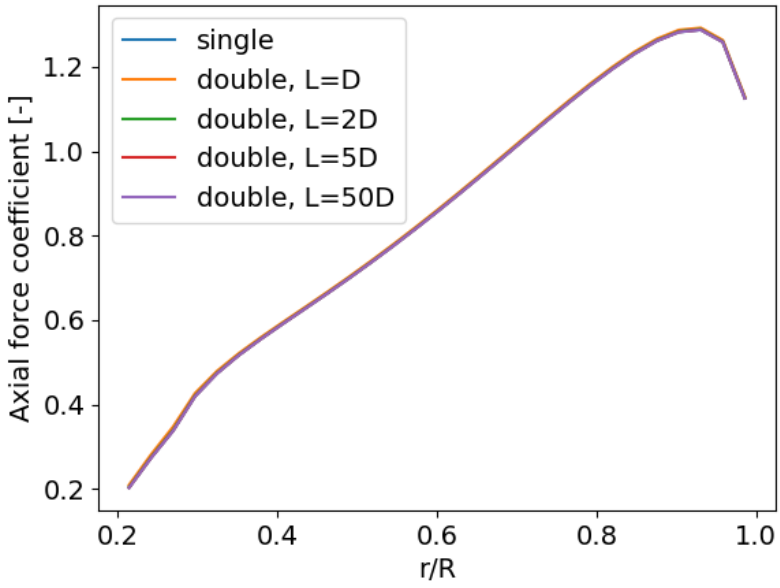

Fig. 11 Comparison of radial distribution of axial load for single and double rotor cases for various L at $\psi = 0$

Just like the previous realisation of an additional rotor in-plane not having a significant effect on the radial distribution of forces regardless of the value of L, additional rotor for various values of ψ also does not have any significant effect on the forces as it is observed from Figure 12 and Figure 13.

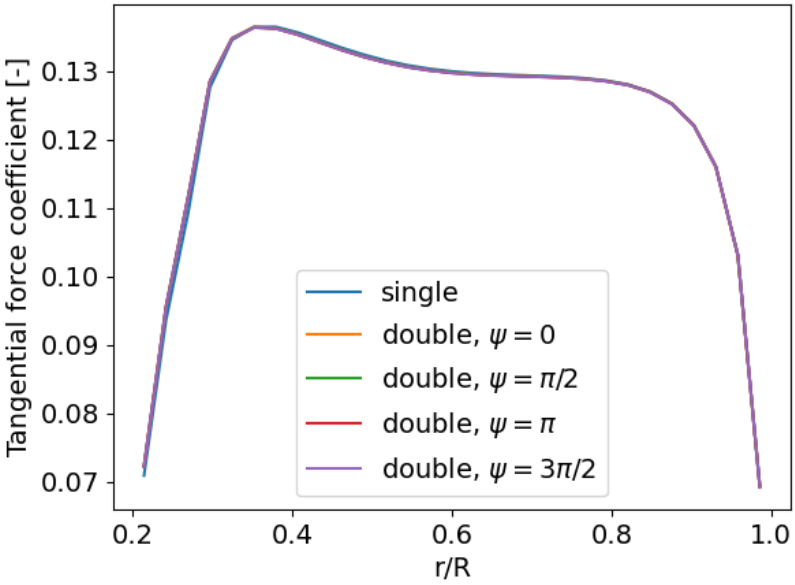

Fig. 12 Comparison of radial distribution of tangential load for single and double rotor cases for various ψ at $L = D$

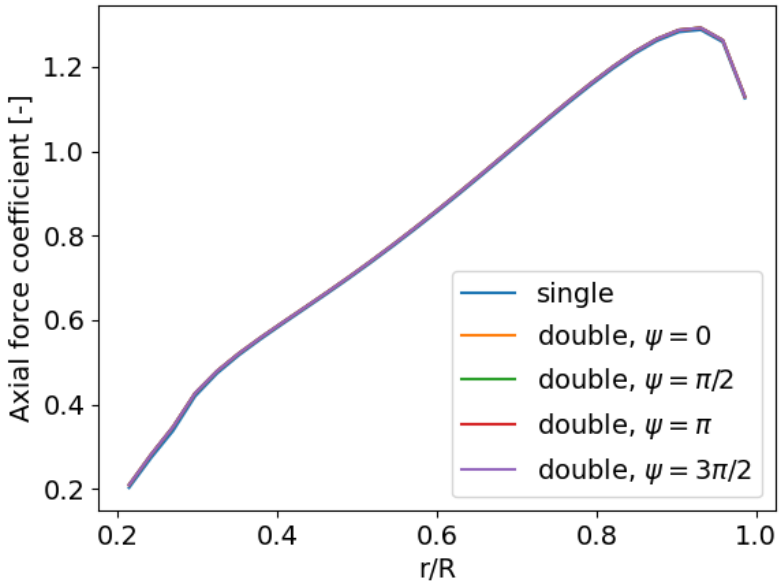

Fig. 13 Comparison of radial distribution of axial load for single and double rotor cases for various ψ at $L = D$

3.5. Total thrust coefficient and power coefficient

The total thrust and power coefficients are calculated as

$$C_T = \frac{B \sum F_a \Delta r}{\frac{1}{2}\rho A U_\infty^2} \tag{3.4}$$

$$C_P = \frac{B\Omega \sum F_t r \Delta r}{\frac{1}{2}\rho A U_\infty^2} \tag{3.5}$$

where A is the rotor area, r is the radial coordinate of each element and dr is the element size. These coefficients are computed and plotted in Figure 14 and Figure 15 for comparison between single and double rotor cases. The result for single rotor case has been presented as a single blue horizontal line across the plot for each figure whereas the double rotor cases are plotted according to the magnitude of L they used in terms of D.

For C_T, it can be observed that for $L = D$, the magnitude differs by a small but still a significant amount. As the value of L increases, the value of C_T approaches that of a single rotor and at $L = 50D$, it exactly overlaps with the single rotor case.

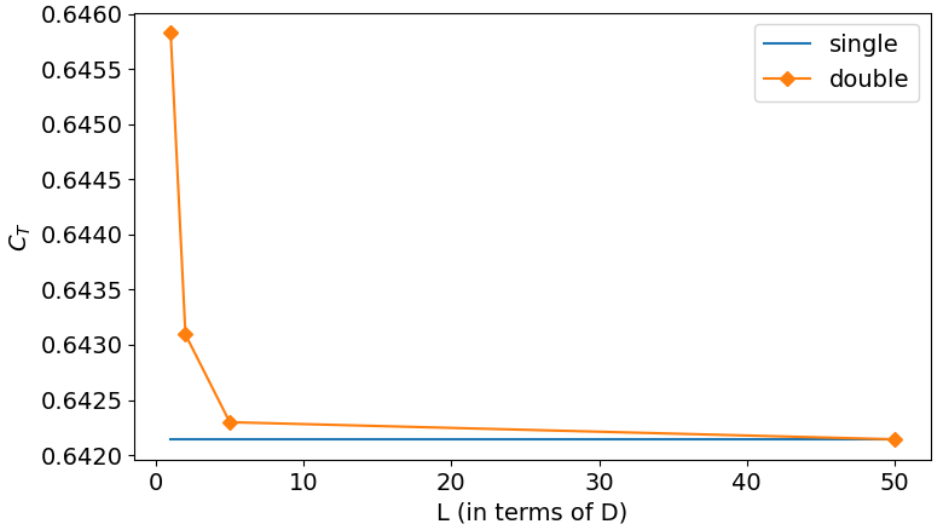

Fig. 14 Comparison of C_T for single and double rotor cases

As for C_P a greater value of L than $50D$ was required to observe the convergence of the double rotor case to the result of the single rotor case. Initially at lower values of $L = D$ and $2D$, the C_P of double rotor case are much lower than the single rotor case and at $L = 5D$, the value overshoots the value of single rotor case. Further increment of L and at about $L = 250D$, the C_P of double rotor case somewhat closes to that of single rotor case. Nevertheless, it can be concluded that for $L \to \infty$, the result for the double rotor case comes close to the single rotor case.

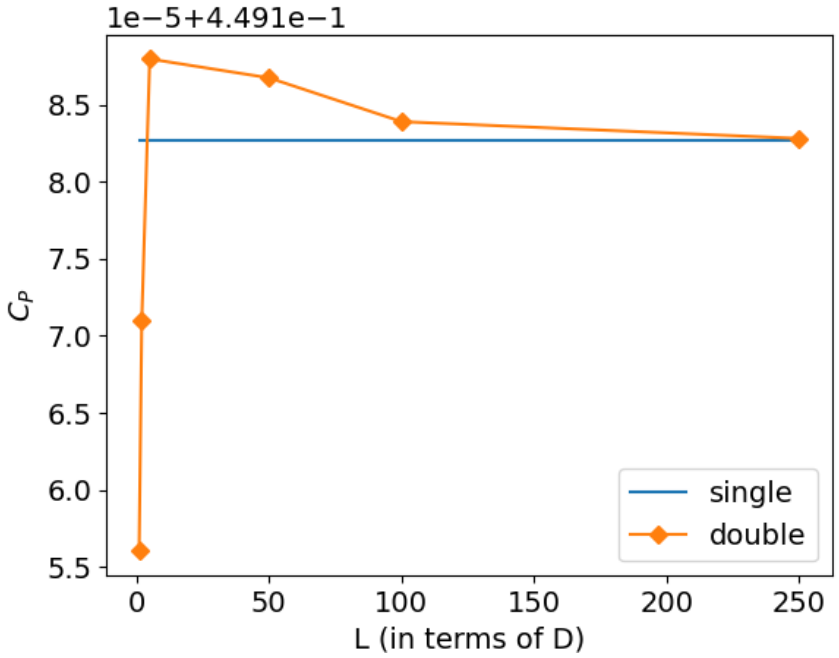

Fig. 15 Comparison of C_P for single and double rotor cases

3.6. Evaluation

The comparisons between the single rotor case and the double rotor case were found to have minimal differences in general. For parameters that have significant differences, these differences decreased exponentially with an increase in distance between the rotors for the double rotor case. Moreover, the small differences were only apparent at the hub of the rotor and the other parts of the rotors on other radial positions seem to be almost unaffected. This comparison was also made for non-zero phase differences between the two rotors of the double rotor case and it was realised that there was no significant effect imposed by the phase difference on the various parameters under study. Thus, the tip effect seems to be independent of the phase differences and is only a function of the distance between the two rotors. Furthermore, the distance required between the rotors is not large to achieve stream tube independence as it was observed that for $L = 2D$, the radial distributions of all the parameters have already or almost overlapping the single rotor case.

4. Comparison between Lifting line model and BEM

4.1. Radial distribution of angle of attack

The angle of attack is plotted against r/R in Figure 16. In this plot, one can see that the angle of attack from lifting line theory matches quite well with that of BEM for $r/R > 0.6$. The high discrepancies are at the root of the blade, where the differences are about six degrees between lifting line and BEM.

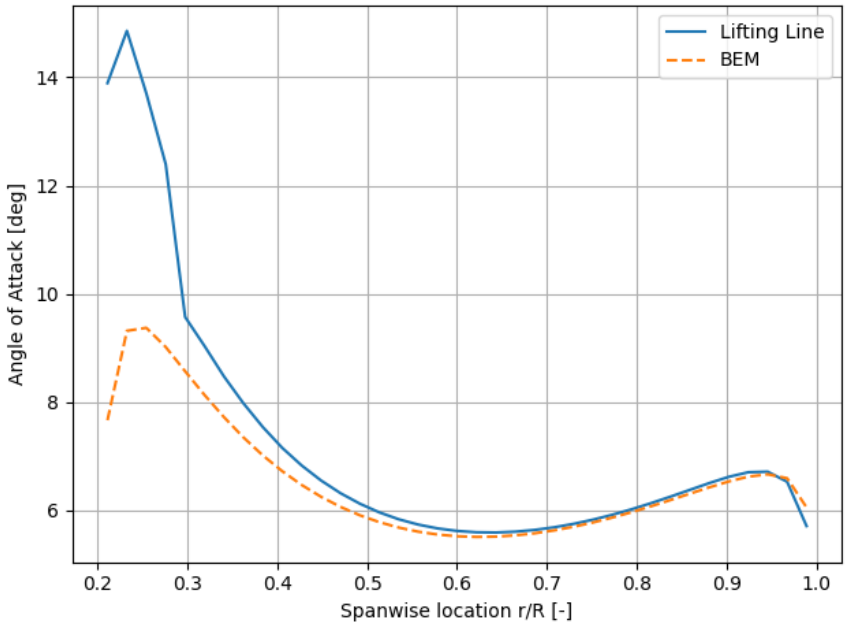

Fig. 16 Comparison of radial distribution of angle of attack for single and double rotor cases

4.2. Radial distribution of inflow angle

When one looks at the radial distribution of the inflow angle in Figure 17, the same discrepancies as for the angle of attack can be seen for the inflow angle at the root. This makes sense since the inflow angle is just a sum of the angle attack and the pitch and twist angle of the blade. The inflow angle that the lifting line theory predicts is well above the stall angle, so the root stalls and it is expected to see a drop in circulation as well.

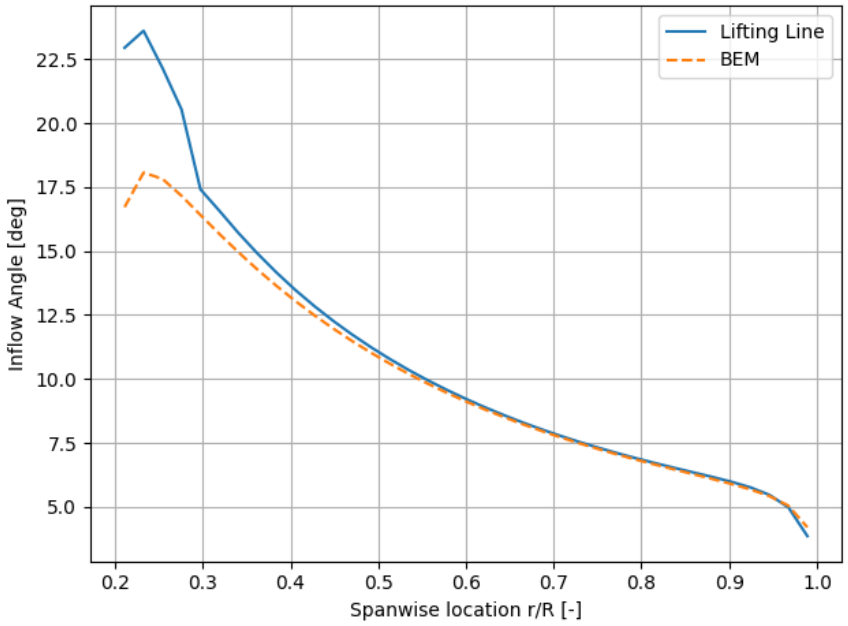

Fig. 17 Comparison of radial distribution of angle of attack for single and double rotor cases

4.3. Radial distribution of circulation

A non-dimensional expression for the circulation is given by (3.1). The circulation is plotted against r/R in Figure 18. Again for values $r/R > 0.6$ lifting line and BEM match quite well. At the root of the blade, the lifting line predicts bigger circulation losses compared to BEM, as was expected from the inflow angle plot. However, this is compensated by lifting line by predicting a larger circulation around $r/R = 0.3$.

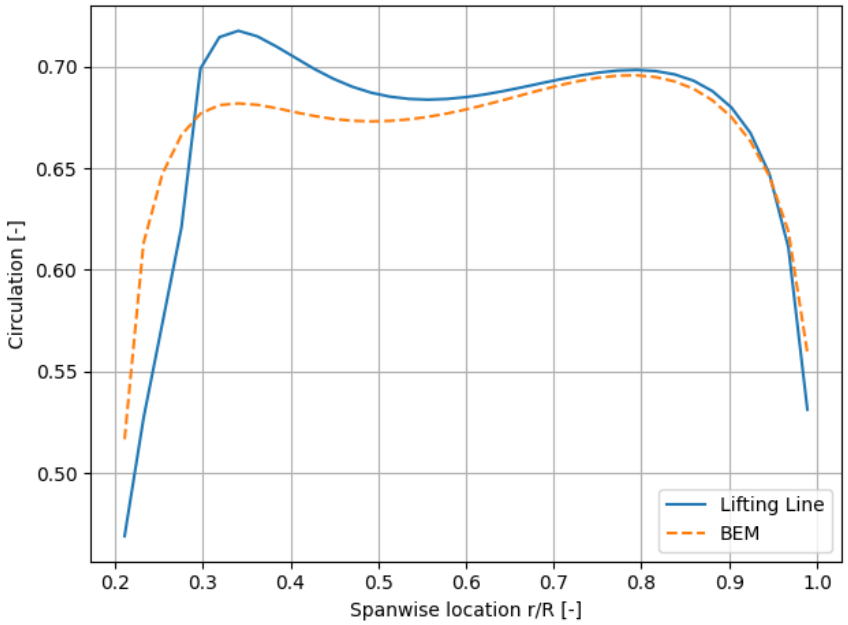

Fig. 18 Comparison of radial distribution of angle of attack for single and double rotor cases

4.4. Radial distribution of tangential load

When comparing the non-dimensional tangential load in Figure 19, the differences are not as big as the previous plots. The values seems to match already quite well after $r/R > 0.5$, but again there are differences at the root. Like in the case for the circulation, lifting line predicts larger losses for $0.2 < r/R < 0.3$, and larger loads for $0.3 < r/R < 0.5$. The non-dimensional expression for the tangential used in this plot is given by (3.2)

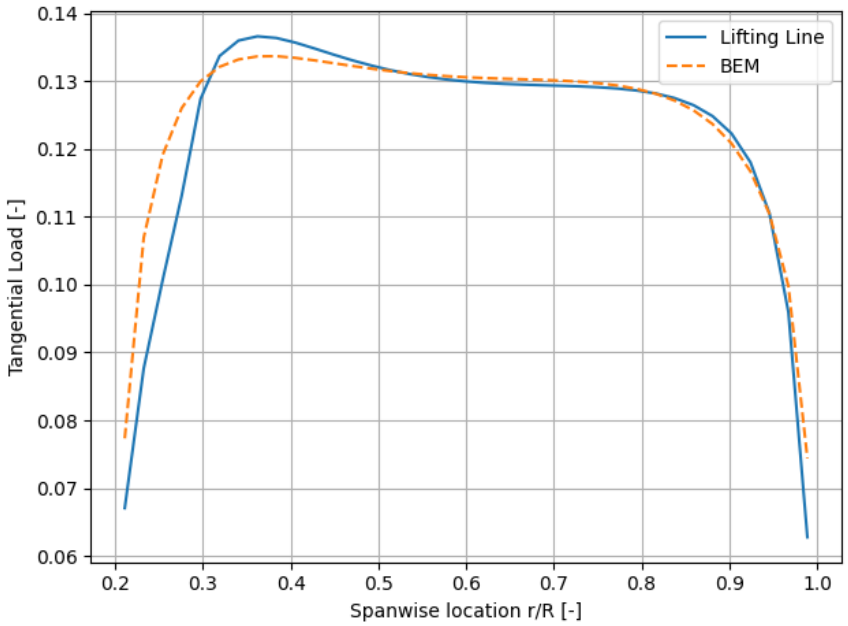

Fig. 19 Comparison of radial distribution of angle of attack for single and double rotor cases

4.5. Radial distribution of axial load

Like it was observed for the tangential load case, a greater axial force at the root is predicted by BEM. Compared to the other parameters plotted before in this section, the axial load seems to match the best when comparing the lifting line and BEM. From Figure 20, it can be seen that after $r/R = 0.3$ the results seems to match almost exactly. The non-dimensionalisation of the axial load is given by (3.3)

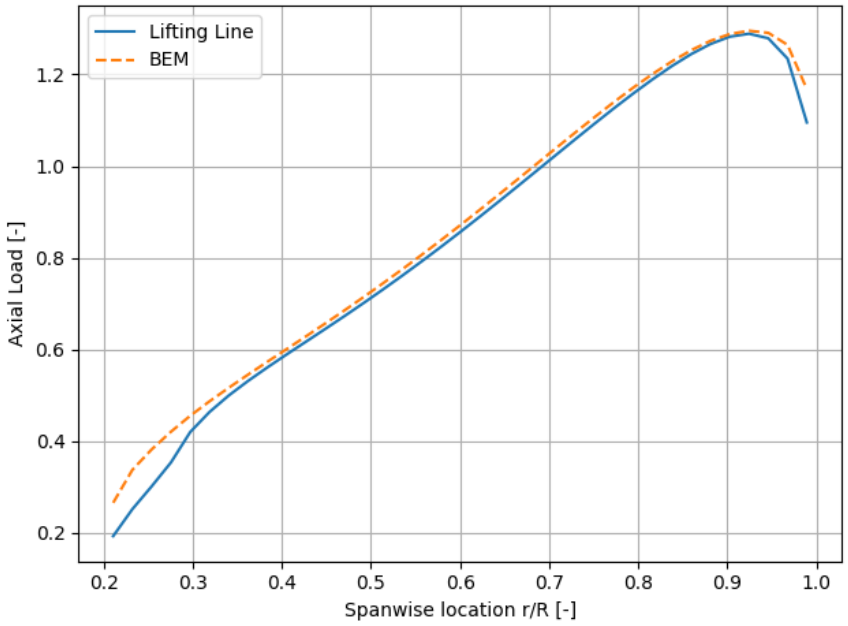

Fig. 20 Comparison of radial distribution of angle of attack for single and double rotor cases

	BEM	Lifting Line
C_T	0.658	0.641
C_P	0.452	0.448

Table 1 Power and thrust coefficient calculated by lifting line and BEM

4.6. Total thrust coefficient and power coefficient

The values for C_P and C_T calculated by lifting line theory and BEM are given in (1). For the C_T the difference in BEM and lifting line is around 1% while for thrust coefficient they are approximately 2.5%.

The thrust coefficient is calculated as given in (3.4), while the power coefficient is calculated as given in (3.5). From these equations, it can be seen that for a fixed blade geometry, operational conditions and freestream conditions, different values for C_P and C_T must be due to differences in axial load and tangential load distributions in the two methods. We already saw from Figure 19 and Figure 20, that there are indeed some differences in the load. The main differences were shown to be at the root. So this would be the main contributor to the difference in the performance parameters between the lifting line and BEM.

5. Sensitivity of results

5.1. Sensitivity to wake advection speed

As mentioned in previous sections, the advection speed of the wake is not a parameter used in the model and is itself iterated until convergence, thus no sensitivity on it needs to be performed. It was tested, that all reasonable initial choices of induction factor resulted in the same converged result, however, a good initial guess can reduce the number of iterations needed for convergence.

5.2. Sensitivity to spacing method

The sensitivity of the results was investigated with respect to the spanwise spacing method. The results can be seen in Figure 21. It can be seen, that the results agree very well with the middle part of the blade. However, with cosine spacing, spurious oscillations can be observed near the root and tip for high values of circulation. This can be attributed to the very small spacing between vortex filaments, leading to extremely high values of induced velocity.

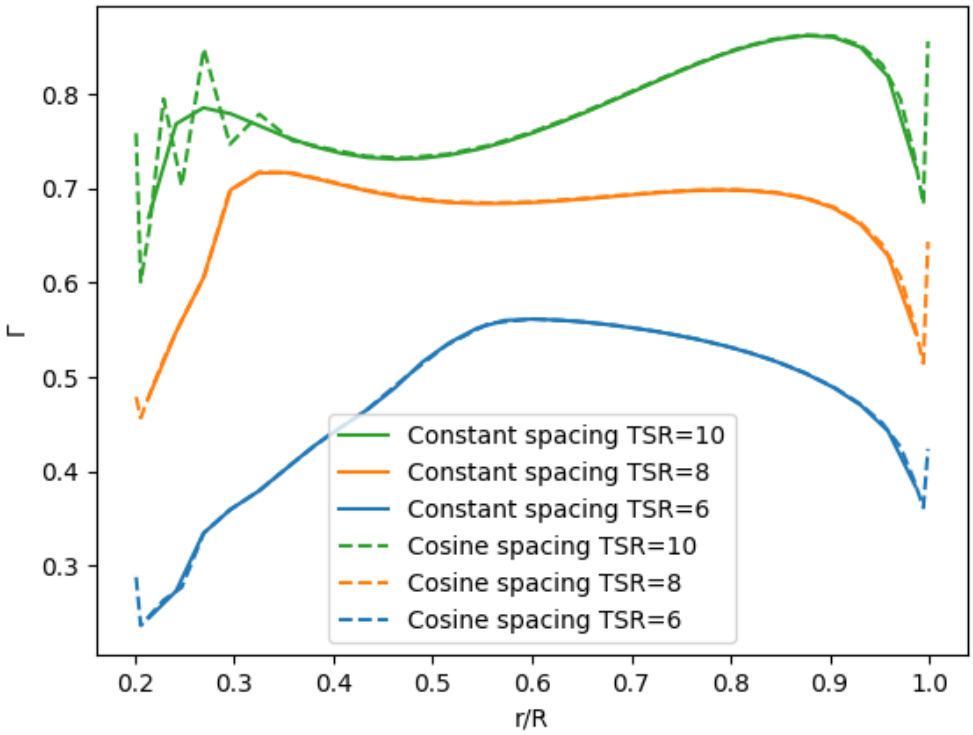

Fig. 21 Comparison of Circulation distribution vs radial position for different TSR and spanwise spacing methods

5.3. Sensitivity to wake discretization

The effect of wake discretization on the element was determined by varying the length of the discrete filaments L_f and comparing the resulting performance of the rotor, which can be seen in Figure 22. ΔC_T is defined as the absolute value of the difference of C_T between the filament length and the filament length of the adjacent datapoint with longer filament length. It can be seen that the values converge with approximately second-order accuracy, which is expected from the midpoint rule used in the integration.

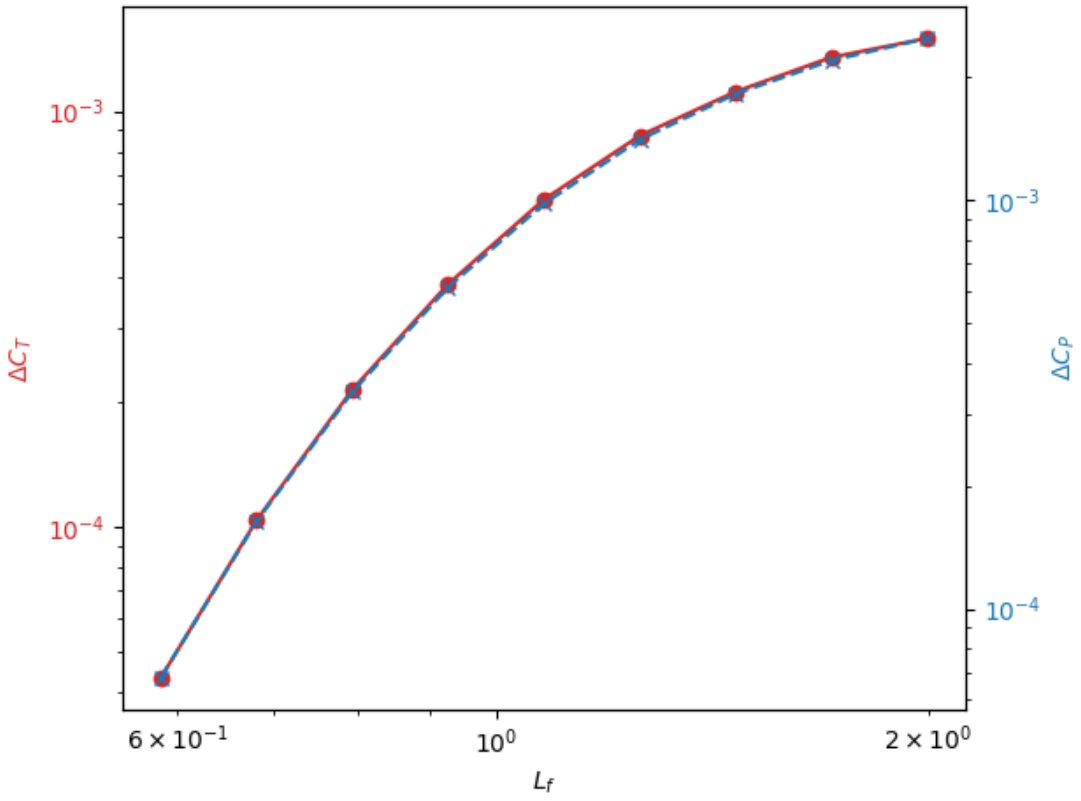

Fig. 22 Comparison of C_T and C_P for different filament element lengths at TSR = 8

5.4. Sensitivity to wake length

The effect of the length of the computed wave was determined by varying the number of wake rotations N_r and computing a similar error norm as in the previous plot. The results can be seen in Figure 23. It can be seen, that the value of C_T and C_P again converges with second-order accuracy compared to the number of wake rotations. For 100 wake rotations, the change in performance is already smaller than the convergence tolerance used in simulations.

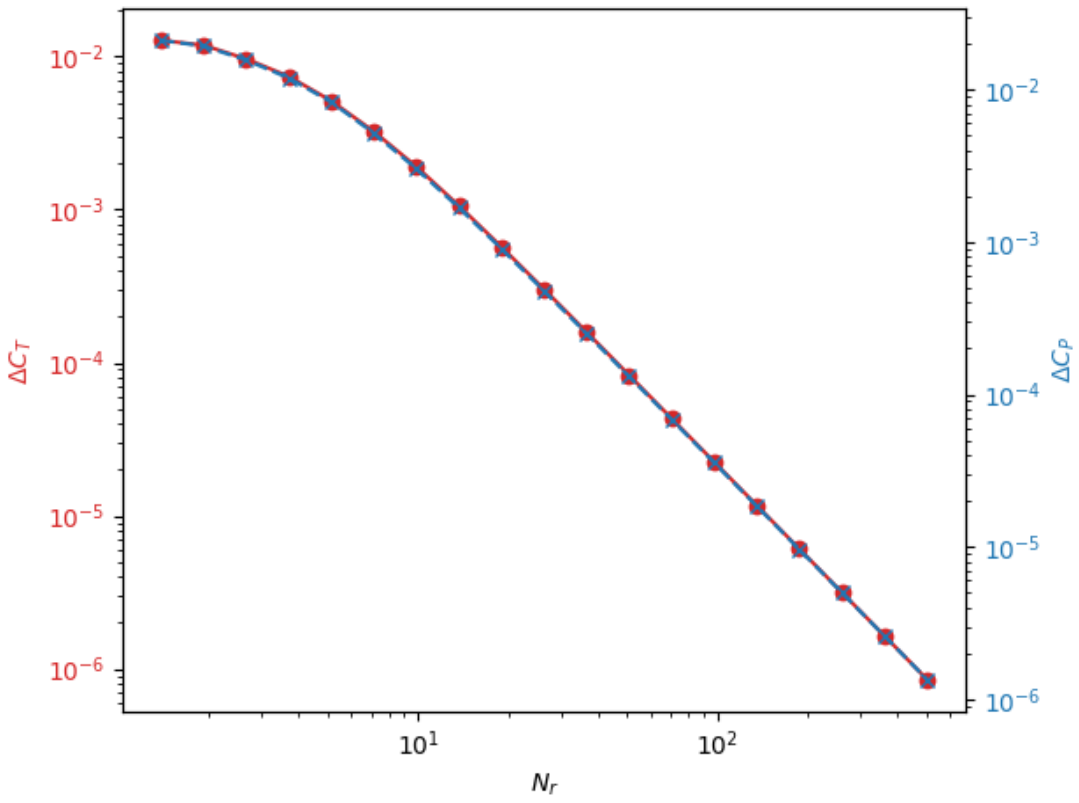

Fig. 23 Comparison of C_T and C_P for different number of wake rotations at TSR = 8

5.5. Effect of multiple rotors on the wake geometry

For multiple rotors, the effect of the secondary wake is taken into account however, the wake geometry for both wakes is frozen and thus not accurately represent reality.

6. Conclusion

The differences in the radial distributions of various parameters between the single rotor case and the double rotor case were found to be minimal in general. If any, the minimal differences were only apparent at the hub of the rotor and these differences exponentially decreased with increasing distance between the two rotors. This comparison was also made for non-zero phase differences between the two rotors of the double rotor case and it was realised that there was no significant effect induced by the phase difference.

On the other hand, large magnitudes of differences can be observed when the lifting line model and BEM were compared. The majority of these large differences were sourced from the hub of the rotor. However, unlike the previous comparison between single and double rotor cases, the differences were also significant and clear in other parts of the rotor such as the midsection and also the tip. Furthermore, these two methods make use of multiple assumptions among which uniform flow speed is a common assumption. As for the contradicting assumptions, BEM uses an empirical method for tip and root losses while the lifting line method does not make use of it. Additionally, BEM uses momentum theory that assumes an actuator disk while the lifting line method merely assumes a finite number of blades.

Lastly for the sensitivity of the results to various parameters such as wake advection speed, spacing method, wake discretization, wake length and the number of rotors on the wake geometry were analysed. Other than the spacing method in which the cosine spacing method showed spurious oscillations near the root and tip, the other parameters were found to not affect the results.